UNIVERSIDADE DE SÃO PAULO

INSTITUTO DE FÍSICA
CAIXA POSTAL 20516
01498 - SÃO PAULO - SP
BRASIL

PUBLICAÇÕES

IFUSP/P-860

EXPLORATORY STUDIES OF THE ELASTIC SCATTERING OF $^{11}Li + ^{12}C$

G.R. Satchler
Physics Division, Oak Ridge National Laboratory
Oak Ridge, TN 37831-6373

K.W. McVoy
Department of Physics, University of Wisconsin
Madison, WI 53706

M.S. Hussein
Instituto de Física, Universidade de São Paulo

Agosto/1990

(to be submitted to Nuclear Physics A)

EXPLORATORY STUDIES OF THE ELASTIC SCATTERING OF $^{11}Li + ^{12}C$

G. R. Satchler
Physics Division
Oak Ridge National Laboratory*
Oak Ridge, TN 37831-6373

K. W. McVoy**
Department of Physics
University of Wisconsin
Madison, WI 53706

and

M. S. Hussein***
Instituto de Fisica
Universidade de São Paulo
CP 20516, São Paulo, Brazil

Abstract:

Calculations have been made of the elastic scattering of $^{11}Li + ^{12}C$ at E/A = 30 and 85 MeV as an example of the scattering to be expected for "exotic" neutron-rich light nuclei. The real optical potential was generated from a folding model using Hartree-Fock densities for ^{11}Li. A variety of assumptions for the absorptive imaginary potential were explored, subject to the important constraint that the predicted reaction cross section remain reasonable. Contrary to some expectations, we provide evidence that these weakly bound systems do not exhibit the diffractive type of scattering that is characteristic of strong absorption. If anything, their more diffuse real potentials can result in an enhancement of the refractive features.

*Operated by Martin Marietta Energy Systems, Inc. under contract DE-AC05-84OR21400 with the U.S. Department of Energy.
**Supported in part by the National Science Foundation.
***Supported in part by the CNPq, Brazil.

1. Introduction

Recently, several groups[1-4] have studied the interactions of secondary beams of radioactive, neutron-rich, light nuclei. In some cases, such as ^{8}He, ^{11}Li and ^{14}Be, the interaction cross sections at E/A = 790 MeV were found[1] to be much larger, compared to those for the stable isotopes, than would be expected from nuclear radii which increased proportionally to $A^{1/3}$. Similar effects were observed[3] for E/A $\lesssim$ 50 MeV. These increases in cross section have been associated with the increasingly weak binding of the excess neutrons[5,6]. The fragmentation of ^{11}Li by a ^{12}C target has also been measured[2]. In the ^{9}Li channel, the momentum distribution of ^{9}Li fragments shows the superposition of a narrow peak on a broad one. The narrow peak has been associated[2,7,8] with the removal of two neutrons from a weakly bound "halo" (two-neutron separation energy = 0.19 ± 0.11 MeV), and the broad one with removal from the more normally bound "core" (separation energy = 6.0 ± 1.5 MeV). The effective mean radius of the halo estimated from these measurements is ~6.5 fm, much larger than the radius of ^{9}Li (~2.5 fm).

Currently, other experiments with these exotic beams are planned at lower energies, E/A ~ 20 to 85 MeV, say. Consequently, it is of some value to consider what might be expected for quasi-elastic processes at these energies. Our purpose here is to discuss elastic scattering angular distributions, based upon plausible assumptions about the corresponding optical potentials. We adopt $^{11}Li + ^{12}C$ scattering at E/A = 30 and 85 MeV as examples.

Recent work[9,10] has established that the elastic scattering of light heavy-ion systems such as $^{12}C + ^{12}C$, $^{16}O + ^{12}C$ and $^{16}O + ^{16}O$ show sufficient transparency for the cross sections to be dominated by farside scattering[11]. In particular, there is often the appearance of a prominent (but damped) rainbow[10,11]. It has been speculated that exotic

nuclei like ^{11}Li would exhibit much stronger absorption because of the weak binding of the excess neutrons so that there would no longer be farside dominance. Then the scattering would be more characteristic of the scattering by a black sphere for which the nearside and farside amplitudes are equal at all angles and their interference produces marked diffractive oscillations[11]. However, we shall show here that there are good reasons to believe that this is not so, and that the scattering is still dominated by refraction.

2. Construction of the optical potential

Here we describe the construction of the complex optical potential, U = V + iW. The real potential was obtained from the folding model, using the DDM3Y effective nucleon-nucleon interaction described elsewhere[9], together with realistic representations of the nuclear density distributions[12]. For ^{11}Li we took the spherical Hartree-Fock densities of Bertsch *et al.*[6] which were shown to account for the interaction cross sections measured at E/A = 790 MeV, while a shell-model density[12] was used for ^{12}C. The DDM3Y interaction is both energy and density dependent, and has successfully described[9] the scattering of stable light heavy-ion systems over a range of energies E/A ≈ 10 to 120 MeV.

The resulting folded potentials $V_F(r)$ for ^{11}Li + ^{12}C and ^{12}C + ^{12}C at E/A = 85 MeV are compared in fig. 1. As expected, the ^{11}Li potential is more diffuse than the ^{12}C one because of the greater radial extent of the ^{11}Li density; the ^{11}Li potential has an RMS radius of 4.38 fm compared to 3.99 fm for ^{12}C. Also shown in fig. 1 is the result of omitting the contributions of the two valence neutrons from the ^{11}Li density distribution. These two neutrons only give rise to about 10% of the folded potential at small radii, but are responsible for almost all of it at large distances (50% at r ≈ 7.5 fm, where the potential is -1 MeV, and 90% at r = 10 fm, for example). The potentials for E/A = 30 MeV are

similar in shape but stronger by 50 to 60%. Their other characteristics are very similar to those shown in fig. 1.

The folding model was "calibrated" by using the ^{12}C + ^{12}C potentials to fit scattering data for this system at the corresponding energies. It was found to be adequate (see fig. 2a) to use the folded shape for both real and imaginary parts of the potential at E/A ≈ 85 MeV, with a complex renormalization factor so that we have $U(r) = (N_R + iN_I)V_F(r)$. However, this assumption was not satisfactory at the lower energy of E/A = 30 MeV, as indicated by the dot-dash curve in fig. 2b. A much better fit to the data at this energy (solid curve) was obtained by using an imaginary potential W(r) of Woods-Saxon shape. In both cases, the renormalization N_R required for the real potential was close to unity.

The loose structure of ^{11}Li allows it to be fragmented more easily than ^{12}C and this could result in some modification of the ^{11}Li + ^{12}C real potential compared to that for ^{12}C + ^{12}C. The analogous break-up of ^{6,7}Li and ^{9}Be has been found[13,14] to contribute a repulsive term to their real potentials and to increase the strength of the absorptive potentials. The possible effects of this for ^{11}Li are explored here at E/A = 30 MeV. However, the explicit calculations[14] for ^{6}Li have shown break-up to be much less important at higher energies of E/A $\gtrsim$ 100 MeV. We assumed this to be true also for the real potential for ^{11}Li, although we did consider the effects of an additional weak absorptive potential of very long range. The possibility of such a term arises because, although the separation energy of a single neutron from ^{11}Li is about 1 MeV, the pair of valence neutrons has a separation energy of only 0.2 MeV. This implies a pairing energy of 0.8 MeV and suggests a cluster model of ^{11}Li as a dineutron very weakly bound to a ^{9}Li core[7]. Such a picture is consistent with the observation[2] of a relatively sharp peak in the

perpendicular momentum distribution of ^{9}Li fragments from ^{11}Li break-up. The absorption from the elastic channel due to this fragmentation could be represented in the optical potential by an imaginary term of exponential form with a range determined essentially[15] by the 2n separation energy of 0.2 MeV; that is, at large r we may use the phenomenological form

$$\Delta W(r) = -W_p \exp(-r/\alpha) \quad (1)$$

with $\alpha \approx 7.98$ fm.

We can place some constraint on variations of the optical potential away from the simple folding model described above by requiring that the predicted reaction cross section σ_A remain "reasonable." Although measurements of $\sigma_A(E)$ for the exotic projectiles are not yet available at the energies considered here, some guidance can be obtained from other measurements.

3. Reaction cross section systematics

First, we note that the cross sections referred to here, measured[1-3] at E/A ~ 1 GeV, are so-called interaction cross sections; that is, that part of the reaction cross section σ_A in which the neutron and/or proton number of the projectile is changed. Hence inelastic excitations are omitted and they underestimate the true reaction cross section which should be compared to an optical model prediction. (The deficiency has been estimated[16] to be about 5%.) This does not seem to be a problem at the lower energies, and measured cross sections can be identified with $\sigma_A(E)$.

3.1. CROSS SECTIONS AT E/A = 85 MEV

The measured[17] and calculated[18] reaction cross sections are found to vary very slowly with energy above E/A ~ 100 MeV, so that the values measured[1] at E/A ~ 1 GeV provide some guide as to their values at E/A = 85 MeV. For example, the interaction cross

section for ^{11}Li + ^{12}C at E/A = 790 MeV was measured[1] to be 1047 ± 40 mb. Since ^{11}Li has no bound excited states, and hence no inelastic scattering, we may identify this with the reaction cross section. The measured[16] value for ^{12}C + ^{12}C at E/A = 870 MeV was 939 ± 40 mb; the value of σ_A may be[16] about 5% larger. Thus the measured ratio for ^{11}Li to ^{12}C is 1.12 ± 0.04, and the ratio of reaction cross sections is probably even closer to unity. Projectile fragmentation, which is facilitated by the weak binding of ^{11}Li, contributes[2] about 40%of its reaction cross section at E/A = 790 MeV. The production of ^{9}Li is responsible for about one-half of this[2]. It is possible that fragmentation may be somewhat more important at E/A = 85 MeV, thus enhancing the reaction cross section for ^{11}Li relative to that for ^{12}C.

The σ_A for ^{12}C + ^{12}C at E/A = 83 MeV has been measured[17] to be 965 ± 30 mb, which is almost unchanged from its value at the much higher energy. If this were also true for ^{11}Li + ^{12}C, we would predict $\sigma_A \approx 1030$ to 1080 mb for this system at E/A = 85 MeV. Even if the ^{11}Li fragmentation cross section were doubled at the lower energy, we would only anticipate $\sigma_A \approx 1500$ mb.

3.2. CROSS SECTIONS AT E/A = 30 MEV

There is more uncertainty at the lower energies where the break-up of loosely bound projectiles becomes more important[13,14]. The average cross sections for a variety of neutron-rich projectiles, over ranges of energies up to 60 MeV per nucleon, and on a target of ^{28}Si, have shown[3] a roughly linear dependence upon their neutron excess, (N-Z). (This has been associated[19] with the diffuseness of the neutron density distribution increasing with neutron excess.) The observed behavior can be represented approximately[3,19] by the relation (for a given A = N+Z),

$$\frac{\sigma_A(N \neq Z)}{\sigma_A(N = Z)} \approx 1.0 + \alpha\,(N - Z), \qquad (2)$$

with $\alpha \approx 0.060 \pm 0.005$.

The measured[17] cross section for $^{12}C + ^{12}C$ at E/A = 30 MeV is $\sigma_A = 1316 \pm 40$ mb. Optical model analyses[9] of the elastic differential cross sections at the same energy imply a value about 70 mb smaller. If the relation (2) is assumed to hold also for ^{12}C as target, it predicts the σ_A for $^{11}Li + ^{12}C$ to be about 30% larger, or about 1710 mb. However, at E/A = 790 MeV, the measured σ_A for ^{11}Li on ^{12}C is about 200 mb larger[1] than a simple extrapolation of the values for the lighter Li isotopes would indicate; this increase has been attributed[6] to the last two neutrons in ^{11}Li occupying the more weakly bound $0p_{1/2}$ orbit. If this increment persists, or is even larger, at the lower energy, we could anticipate a reaction cross section of as much as 2 b for $^{11}Li + ^{12}C$ at E/A = 30 MeV.

4. Optical model predictions

4.1. BOMBARDING ENERGY OF E/A = 85 MEV

Figure 2a shows a fit to the scattering data[20] for $^{12}C + ^{12}C$ at this energy, using the corresponding folded potential multiplied by N = (1.175 + 0.725i). The calculated reaction cross section is 1000 mb, compared to the value 965 ± 30 mb measured[17] at E/A = 83 MeV. The same complex renormalization factor N was then applied to the folded potential for $^{11}Li + ^{12}C$. The calculated scattering for the two systems, in ratio to the corresponding Rutherford cross sections, is compared in fig. 3. The predicted σ_A = 1197 mb for ^{11}Li is 20% larger than for ^{12}C as the projectile.

The most noticeable feature of the comparison of the $\sigma/\sigma_R(\theta)$ ratios for ^{11}Li and ^{12}C in fig. 3 (solid and dotted curves, respectively) is the considerably enhanced ratio for ^{11}Li. However, this is somewhat misleading because the Rutherford cross sections for $^{12}C + ^{12}C$ are four times larger than those for $^{11}Li + ^{12}C$ simply because of the greater charge on

^{12}C. Consequently, the cross sections themselves for the two systems are similar in magnitude over most of the angular range shown. In both cases, we see farside dominance[11] beyond about 5°.

The scattering of ^{11}Li at the larger angles may be damped by increasing the imaginary strength N_I; for example, doubling it (N_I = 1.45) gives σ_A = 1474 mb, which we concluded above might be close to a reasonable upper limit for the expected value at this energy. The farside scattering amplitude is reduced more by the increase in absorption than is the nearside one, consequently they become closer in magnitude and the farside/nearside interference structure seen in the angular distribution (dash-dot curve in fig. 3) is enhanced.

Simply increasing N_I increases σ_A while preserving the shape of the imaginary potential. However, it may seem more reasonable that ^{11}Li scattering is characterized by an imaginary potential of longer range than for ^{12}C. One such possibility is to add a surface-peaked, long-ranged absorptive term, which easily increases the reaction cross section. For example, the use of a Woods-Saxon-derivative imaginary term with a peak magnitude of 1 MeV, radius 6 fm and diffuseness 1.5 fm increases σ_A by 32% to 1576 mb. However, the effect on the elastic angular distribution is much less marked, being more like a uniform reduction by about 30% for $\theta > 5°$, with almost no change in shape.

The extreme in long-ranged absorption is provided by the model of eq. (1). We found, for example, that adding such a term with a strength of W_p = 400 keV to the folded potential with N = (1.175 + 0.725i) increased σ_A from the "bare" value of 1197 mb to 1859 mb. This implies over 600 mb of $^{11}Li \rightarrow {}^{9}Li + n^2$ break-up from this cluster configuration, which seems excessive. Nonetheless, the effect on the elastic angular distribution is negligible! The reason for the apparent paradox is that this term predominantly produces absorption from very high partial waves, and thus very large

impact parameters, which contribute to small scattering angles. A few percent reduction in the ratio to Rutherford is difficult to observe at these angles, but can correspond to a large absorption because the Rutherford cross section is very large there.

We conclude that the elastic differential cross sections for $^{11}Li + ^{12}C$ at E/A = 85 MeV probably lie between the two curves shown in fig. 3, and exhibit refractive features as strong as $^{12}C + ^{12}C$ scattering at the same energy.

4.2. SCATTERING AT E/A = 30 MeV

Figure 2b shows fits to $^{12}C + ^{12}C$ data[20] at this energy. The best fit obtained by assuming the imaginary potential to have the same folded shape as the real one (dotted curve) requires a renormalization by N = 0.842 + 0.573i and is not satisfactory. A superior fit (solid curve) is obtained with N_R = 0.814 and a Woods-Saxon imaginary potential with W_0 = 18.2 MeV, r_W = 1.158 fm and a_W = 0.584 fm. This imaginary potential is less diffuse than the folded one.

The corresponding real and imaginary potentials were constructed for $^{11}Li + ^{12}C$ and their radial shapes are compared in fig. 4. The scatterings predicted for ^{11}Li and ^{12}C are compared in fig. 5. The scattering obtained for ^{11}Li when the same folded shape for the real and imaginary parts (with N = 0.842 + 0.573i) is used is also shown in fig. 5, and results in greater absorption (σ_A = 1469 mb) than when a Woods-Saxon imaginary shape with the same parameters as $^{12}C + ^{12}C$ is used (σ_A = 1230 mb). Again, the ratio to Rutherford for ^{11}Li is ~4 times greater than for ^{12}C at small angles because of its smaller charge. It is even larger for $25° > \theta > 10°$ when the Woods-Saxon imaginary part is used, indicating enhanced farside dominance[11] compared to the $^{12}C + ^{12}C$ case. Also, an interesting dip appears in the angular distribution near 30° in this case (solid curve in fig.

5). A nearside/farside decomposition[11] shows that this is an Airy minimum in the farside scattering. It can be made much more prominent by increasing W_0 from 18.2 to 24 MeV. However, the minimum is removed by the very much stronger absorption at small radii that occurs with the use of the folded shape for the imaginary potential. (The latter reaches a strength of -97i MeV at r = 0 when N_I = 0.573, compared to the -18.2i MeV for the Woods-Saxon one.)

It was argued in sec. 3.2 above that the reaction cross section for $^{11}Li + ^{12}C$ at this energy might be as large as 2 b. Increasing the imaginary Woods-Saxon strength W_0 is not an efficient way of increasing σ_A; doubling W_0 to 36 MeV only increases σ_A about 15%, to 1411 mb, but has a large effect on the angular distribution. The ratio $d\sigma/d\sigma_R(\theta)$ is reduced considerably for $\theta > 10°$ and oscillations are introduced. However, it seems more plausible, because of the more diffuse density distribution of ^{11}Li, that the Woods-Saxon diffuseness, rather than its strength, should be increased from that appropriate for ^{12}C. Using a_W = 1.0 fm raises σ_A by 40% to 1714 mb; it also has an interesting effect on the angular distribution (see fig. 6). The cross sections are reduced considerably between 6° and 22° but then the residual Airy minimum seen previously near 30° is removed and replaced by a smooth fall-off.

The *ad hoc* introduction of a very diffuse surface absorption term (chosen to have the shape of the derivative of a Woods-Saxon potential) can easily increase σ_A. For example, one with a peak strength of W_D = 2 MeV centered at R_D = 6 fm (r_D = 1.33 fm) and with a_D = 1.5 fm gives σ_A = 2193 mb. However, the effect on the elastic angular distribution (fig. 6) is not dramatic, consisting essentially of a reduction in magnitude of $d\sigma/d\sigma_R(\theta)$ by about a factor of 3 for $\theta > 5°$. (We note that it still has a more "refractive" appearance than that for $^{12}C + ^{12}C$ and a residue of the Airy minimum near 30° remains.)

The extreme of a long-ranged absorptive term is represented by the cluster break-up form of eq. (1). The increment in σ_A that this produces is closely proportional to the strength W_p. The choice W_p = 285 keV gives σ_A = 2 b, but, just as at E/A = 85 MeV, it has no noticeable effect on the elastic angular distribution.

It is possible that fragmentation of ^{11}Li makes the real optical potential significantly less attractive at this lower energy[13,14]. We explored the kind of effects this might have by reducing the strength of the folded real potential by 30% (using a renormalization factor N_R = 0.57 instead of the N_R = 0.814 obtained from the fit to the ^{12}C + ^{12}C data). Two examples are shown in fig. 7, both using the Woods-Saxon imaginary potential, one with the same imaginary parameters as for ^{12}C + ^{12}C and the other with a_W increased to 1.0 fm. The reaction cross sections are almost unchanged from the values obtained using the full N_R = 0.814, but there are large effects on the angular distributions. Simply reducing the real potential by 30% introduces a deep minimum near 22° as well as more interference structure at other angles. A nearside/farside decomposition[11] for this case shows that the sharp dip near 22° is again an Airy minimum in the farside scattering. Indeed, by slowly reducing N_R, one can see that it is the same one that is seen near 30° with the full N_R = 0.814, but the angle at which it occurs has moved forward as the real potential strength is reduced. By chance, the choice of N_R = 0.57, in conjunction with this imaginary potential, is close to maximizing the destructive interference between the inner and outer contributions that give rise to the Airy structure of the rainbow[11]. It would be very interesting to see whether the actual scattering of ^{11}Li + ^{12}C in this energy region reveals any structures like these.

The angular distribution resulting from both reducing N_R by 30% and increasing the imaginary diffuseness to a_W = 1.0 fm has a more conventional appearance (fig. 7) and no sign remains of the Airy minimum. However, comparison with the dot-dashed curve in fig. 6 shows that use of the smaller N_R value has had a large effect here also. Clearly the scattering at this energy is very sensitive to the real potential.

In summary, we see that we can make predictions for ^{11}Li + ^{12}C scattering at this energy with much less confidence, although our calculations help to delineate the kind of features to look for when measurements are made. In particular, it is important to have some measure of the behavior of the cross sections at larger angles (>15°, say) where they begin to fall into the shadow region, and where we have seen the possibility of some distinctive rainbow features occurring.

4.3. CONTRIBUTIONS FROM THE VALENCE OR "HALO" NEUTRONS

One is tempted to think of the excess neutrons, especially the two valence ones that occupy the $0p_{1/2}$ orbital in the Hartree-Fock description[6], as forming a "halo" around a more compact core nucleus. While it is true that the neutron distribution extends to much larger radii than the proton one (see ref. [21] for example), so that the RMS radii are 3.08 and 2.21 fm respectively, it is not obvious how to identify the "halo" component unambiguously. An operational definition might be provided by the momentum measurements[2] on ^{9}Li fragments which imply two groups of neutrons in ^{11}Li. It is natural to identify the group with a narrow momentum distribution, and hence associated with the larger radial extent, with the two most weakly bound valence neutrons. We made this assumption and recalculated the folded potential by omitting these two neutrons from the ^{11}Li density distribution. Using only the (real and imaginary) potential generated by the remaining nine nucleons, with the same N = 1.175+0.725i, has little effect on the ^{11}Li + ^{12}C scattering at E/A = 85 MeV, except for reducing the reaction cross section by 16% and

"stretching" the angular distribution out in angle slightly. The latter effect reflects the smaller radius (RMS radius = 4.01 fm) of the folded potential obtained when only the nine core nucleons are included, compared to when the full density is used (RMS radius = 4.315 fm).

As we have seen (for example, fig. 7), the scattering at E/A = 30 MeV is more sensitive to changes in the real potential. Omitting the valence neutron contributions to the folded potential produces a similar stretching of the Fraunhofer oscillations in the angular distribution as observed at the higher energy, but the reduced attraction also results in generally smaller cross sections at the larger angles (fig. 8). Also, the reduced attraction has the effect of moving the Airy minimum forward from 30° to about 26°.

The calculations shown in fig. 8 were made using the Woods-Saxon imaginary potential obtained from the fit to $^{12}C + ^{12}C$ scattering, but similar effects of omitting the valence contribution to the real potential are seen whatever the choice of imaginary potential. On the other hand, the magnitudes of the reaction cross sections are changed by two percent or less.

It appears that it is not possible to obtain any clear signature of an extended neutron halo by the study of the elastic differential cross sections. The effects of the two valence neutrons are small at the higher energy, while their contribution to the real potential produces changes at the lower energy that are comparable to other uncertainties in our predictions.

5. Conclusions

Our predictions for the scattering of $^{11}Li + ^{12}C$ are somewhat uncertain, but they should help to delineate the kind of features to be sought when measurements are made. The primary positive result is that no support was found for speculations that the break-up of light, neutron-rich nuclei would make their elastic scattering take on the diffractive

characteristics of strong-absorption scattering. It was important in reaching this conclusion that reasonable constraints were placed upon the size of the reaction cross section that was allowed.

The interpretation of this finding is that the additional refraction in the surface region attendant upon the larger extent of the excess neutrons more than compensates for the extra absorption that is allowed. Thus the elastic scattering tends to remain farside-dominated[11].

The scattering at E/A = 30 MeV can be very sensitive to the real potential strength and its relation to the imaginary one. Under some circumstances (e.g., fig. 7), we found a dramatic Airy minimum appearing in the angular distribution. This would provide a good probe of the optical potential if present in the actual scattering of these ions.

The possibility of a very long-ranged absorptive tail due to the fragmentation of a $^{9}Li + 2n$ cluster configuration was found to be very effective in increasing the predicted reaction cross section, but had very little effect on the elastic scattering angular distribution.

We are indebted to A. Brown and G. F. Bertsch for providing the Hartree-Fock densities for ^{11}Li. The calculations were performed using the program PTOLEMY[22].

References

1) I. Tanihata *et al.*, Phys. Rev. Lett. **55** (1985) 2679; Phys. Lett. **B160** (1985) 380, **B206** (1988) 592; Nucl. Phys. **A488** (1988) 113c
2) T. Kobayashi *et al.*, Phys. Rev. Lett. **60** (1988) 2599; Phys. Lett. **B232** (1989) 51
3) W. Mittig *et al.*, Phys. Rev. Lett. **59** (1987) 1889
4) F. D. Becchetti *et al.*, Phys. Rev. **C40** (1989) 1104, and to be published
5) H. Sato and Y. Okuhara, Phys. Lett. **B162** (1985) 217
6) G. F. Bertsch, B. A. Brown and H. Sagawa, Phys. Rev. C39 (1989) 1154
7) C. A. Bertulani and M. S. Hussein, Phys. Rev. Lett. **64** (1990) 1099
8) J. J. Kolata, private communication
9) M. E. Brandan, Phys. Rev. Lett. **60** (1988) 784;
   M. E. Brandan and G. R. Satchler, Nucl. Phys. **A487** (1988) 477;
   A. M. Kobos, M. E. Brandan and G. R. Satchler, Nucl. Phys. **A487** (1988) 457
10) E. Stiliaris *et al.*, Phys. Lett. **B223** (1989) 291
11) M. S. Hussein and K. W. McVoy, Prog. Part. Nucl. Phys. **12** (1984) 103;
   K. W. McVoy and G. R. Satchler, Nucl. Phys. **A417** (1984) 157
12) G. R. Satchler, Nucl. Phys. **A329** (1979) 233
13) Y. Sakuragi, M. Yahiro and M. Kamimura, Prog. Theor. Phys. **70** (1983) 1047;
   Y. Hirabayashi, S. Okabe and Y. Sakuragi, Phys. Lett. **B221** (1989) 227
14) Y. Sakuragi, Phys. Lett. **B220** (1989) 22; T. Yamagata *et al.*, Phys. Rev. **C39** (1989) 873
15) L. F. Canto, R. Donangelo and M. S. Hussein, to be published
16) J. Jaras *et al.*, Phys. Rev. **C18** (1978) 2273
17) S. Kox *et al.*, Phys. Rev. **C35** (1987) 1678
18) J. C. Peng, R. M. DeVries and N. J. DiGiacomo, Phys. Lett. **B98** (1981) 244;
   M. A. Wei-hsing *et al.*, Nucl. Phys. **A477** (1988) 713

19) Shen Wen-qing *et al.*, Nucl. Phys. **A491** (1989) 130
20) M. Buenerd *et al.*, Nucl. Phys. **A424** (1984) 313
21) Y. Tosaka and Y. Suzuki, Nucl. Phys. **A512** (1990) 46
22) M. H. Macfarlane and S. C. Pieper, Argonne National Laboratory report ANL-76-11 (1978)

Figure Captions

Fig. 1. Comparison of the unrenormalized (N = 1.0) folded potentials for $^{11}Li + ^{12}C$ and $^{12}C + ^{12}C$, using the DDM3Y effective nucleon-nucleon interaction for E/A = 85 MeV. Also shown is the potential obtained when the two "valence" neutrons are omitted from the ^{11}Li density distribution.

Fig. 2. (a) Fit to the measured[20] elastic cross sections for $^{12}C + ^{12}C$ at E/A = 85 MeV, using the folded potential of fig. 1 times N = 1.175 + 0.725i. The corresponding reaction cross section is σ_A = 1000 mb. (b) Fits to the measured[20] elastic cross sections for $^{12}C + ^{12}C$ at E/A = 30 MeV. The potential used for the full curve had the folded potential times N = 0.814 for the real part and a Woods-Saxon imaginary part (W_0 = 18.2 MeV, r_W = 1.158 fm, a_W = 0.584 fm). The dot-dash curve is the best fit obtained using the folded shape for both real and imaginary parts, with N = 0.842 + 0.573i. The corresponding reaction cross sections are 1236 and 1214 mb, respectively.

Fig. 3. Elastic cross sections predicted for $^{11}Li + ^{12}C$ at E/A = 85 MeV, using the folded potential in fig. 1 times N = 1.175 + 0.725i (solid curve) and 1.175 + 1.45i (dash-dot curve), shown in ratio to the Rutherford cross sections for this system. The corresponding reaction cross sections are 1197 and 1474 mb, respectively. Also shown for comparison (dotted curve) is the best fit to the $^{12}C + ^{12}C$ data from fig. 2a. (Note that the Rutherford cross sections for $^{12}C + ^{12}C$ are approximately four times larger than those for $^{11}Li + ^{12}C$.)

Fig. 4. The unrenormalized (N_R = 1.0) folded potential for $^{11}Li + ^{12}C$ at E/A = 30 MeV. Also shown is the Woods-Saxon imaginary potential for $^{11}Li + ^{12}C$ using the parameter values obtained from fitting $^{12}C + ^{12}C$ data (fig. 2b).

Fig. 5. Elastic cross sections predicted for $^{11}Li + ^{12}C$ at E/A = 30 MeV, using the folded potential in fig. 4 times N = 0.814, plus the imaginary potential shown there (solid curve), shown in ratio to the Rutherford cross sections for this system. Also shown (dot-dash

curve) is the result of using the folded shape for both real and imaginary parts, with renormalization N = 0.842 + 0.573i. The corresponding reaction cross sections are 1230 and 1469 mb, respectively. The best fit (dotted curve) to the $^{12}C + ^{12}C$ data is also given for comparison. (Note that the Rutherford cross sections for $^{12}C + ^{12}C$ are approximately four times larger than for $^{11}Li + ^{12}C$.)

Fig. 6. The effect on $^{11}Li + ^{12}C$ scattering at E/A = 30 MeV of increasing the absorption. The solid curve is the same as in fig. 5, while the dash-dot curve has the imaginary diffuseness increased to a_W = 1.0 fm. The dotted curve shows the effect of adding a surface absorption term; a Woods-Saxon-derivative with W_D = 2 MeV, R_D = 6 fm and a_D = 1.5 fm was used.

Fig. 7. The effect on $^{11}Li + ^{12}C$ scattering at E/A = 30 MeV of reducing the strength of the real potential by 30%. The solid curve is the same as in fig. 5 (N = 0.814) while the dash-dot curve shows the effect of reducing N to 0.57 without changing the imaginary potential. The dotted curve was obtained by also increasing the imaginary diffuseness to a_W = 1.0 fm.

Fig. 8. The effect on the scattering of $^{11}Li + ^{12}C$ at E/A = 30 MeV of omitting the two valence neutrons of ^{11}Li when constructing the real folded potential.

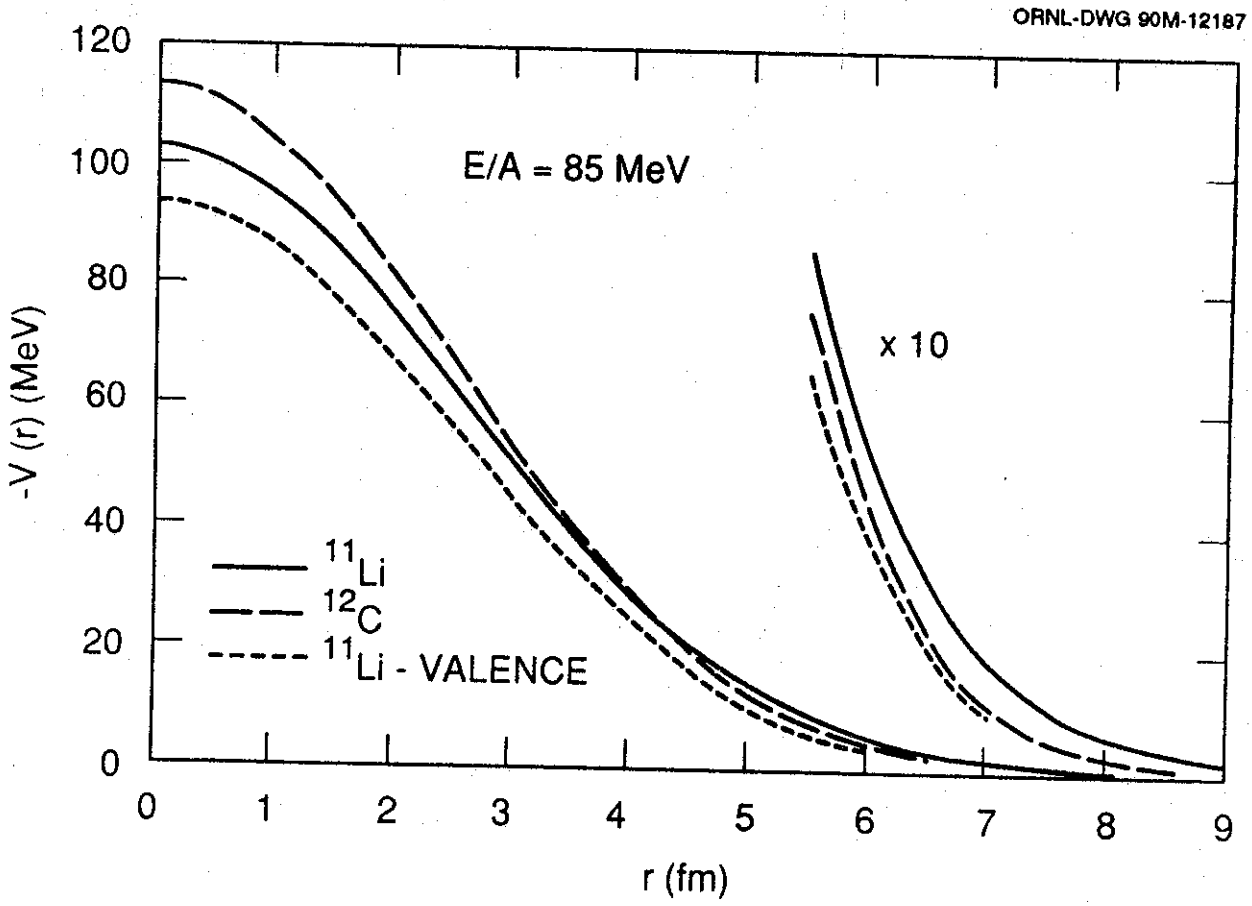
ORNL-DWG 90M-12187
E/A = 85 MeV
x 10
^{11}Li
^{12}C
^{11}Li - VALENCE
-V (r) (MeV)
r (fm)
0
20
40
60
80
100
120
0
1
2
3
4
5
6
7
8
9

Fig. 1

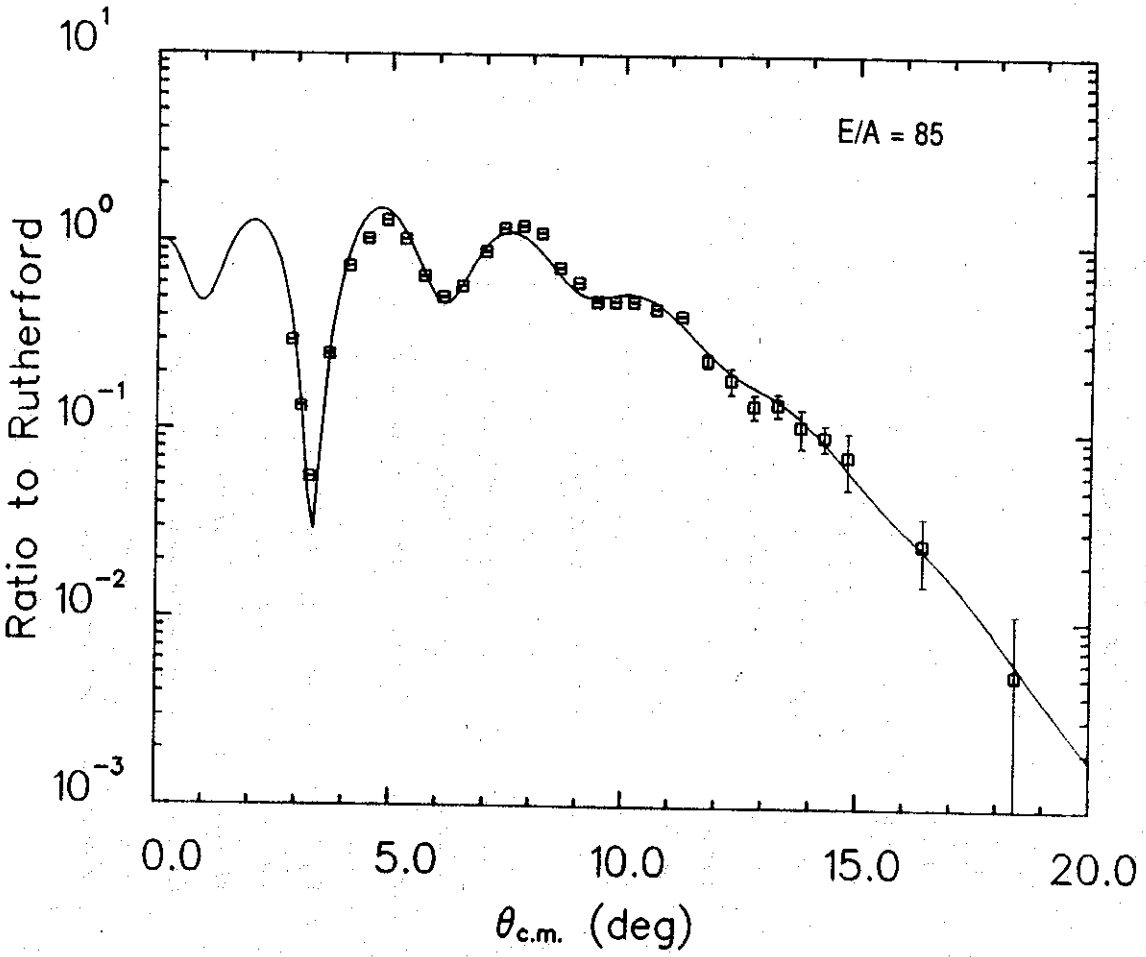
E/A = 85
Ratio to Rutherford
$\theta_{c.m.}$ (deg)
10^{1}
10^{0}
10^{-1}
10^{-2}
10^{-3}
0.0
5.0
10.0
15.0
20.0

Fig. 2a

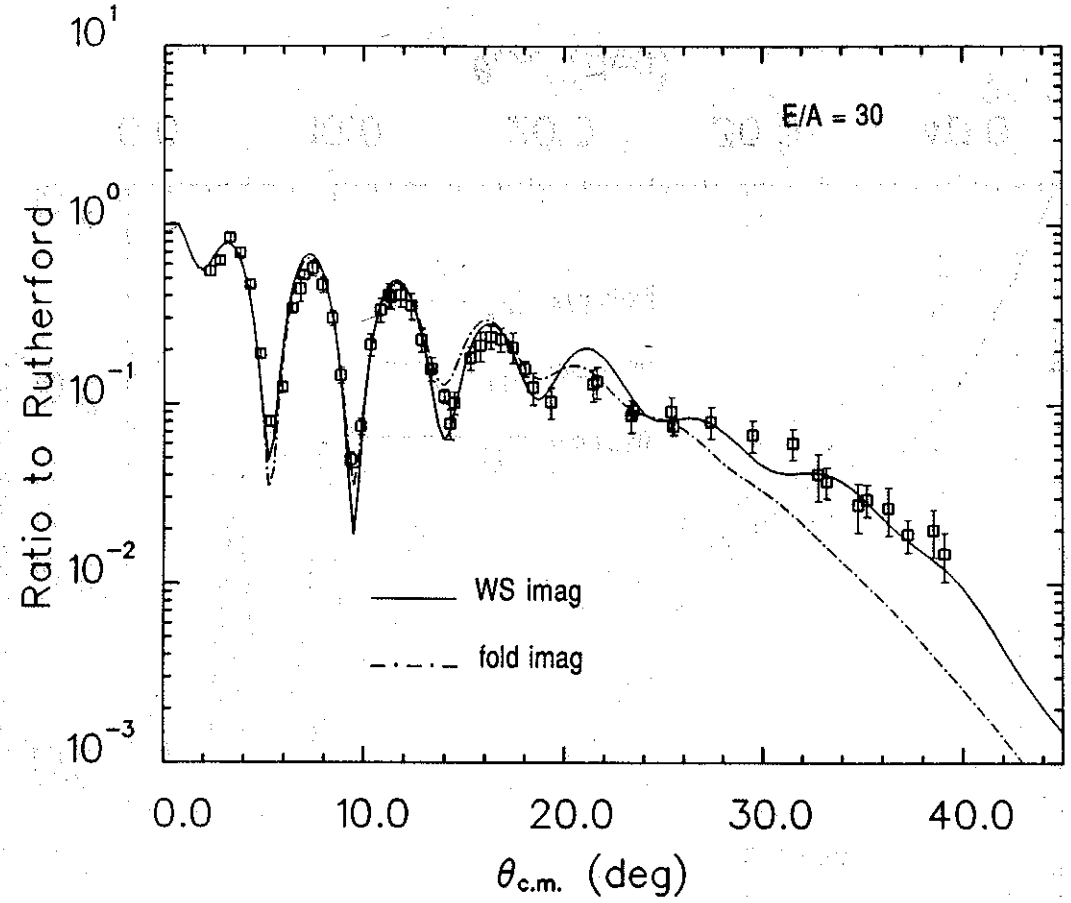
E/A = 30
Ratio to Rutherford
WS imag
fold imag
$\theta_{c.m.}$ (deg)

Fig. 2b

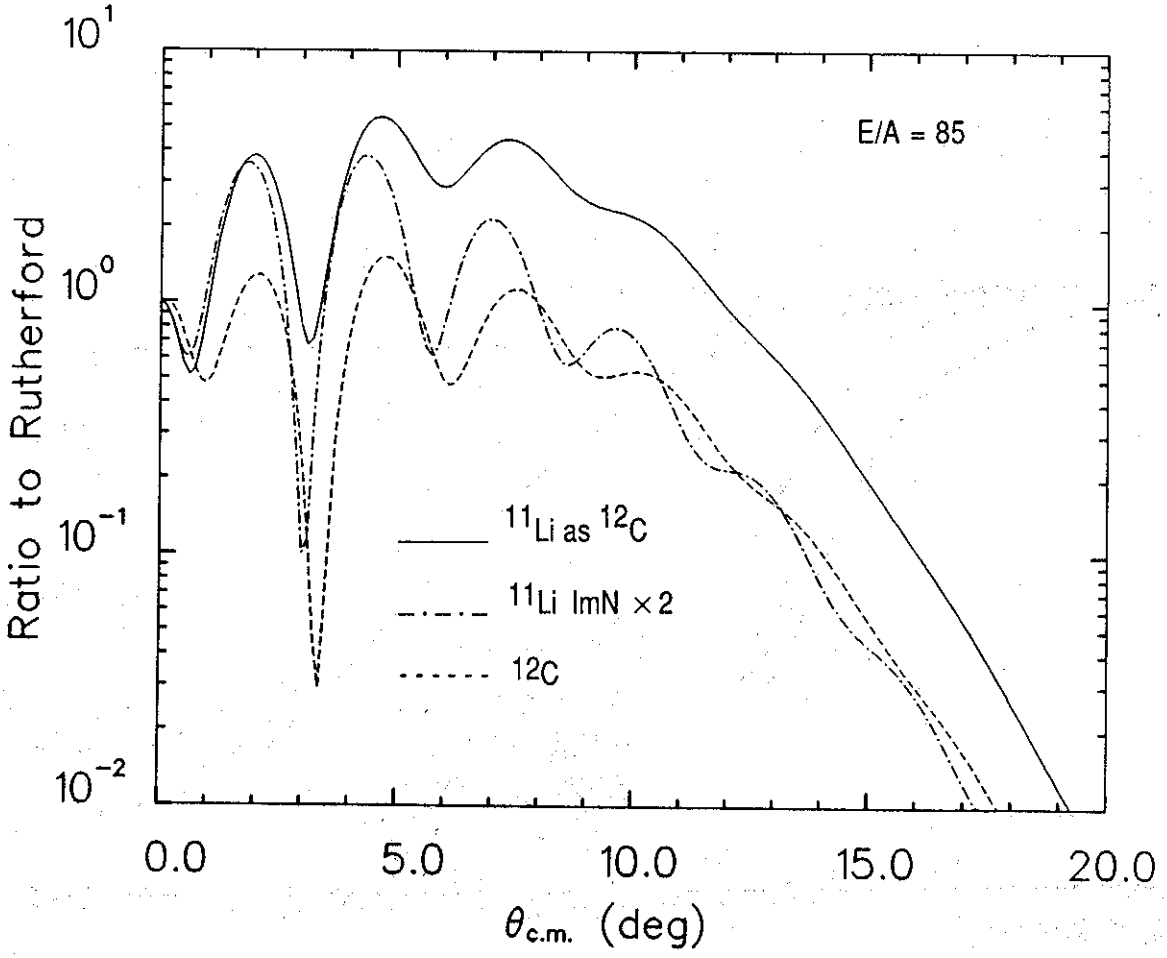
E/A = 85
Ratio to Rutherford
^{11}Li as ^{12}C
^{11}Li ImN ×2
^{12}C
$\theta_{c.m.}$ (deg)

Fig. 3

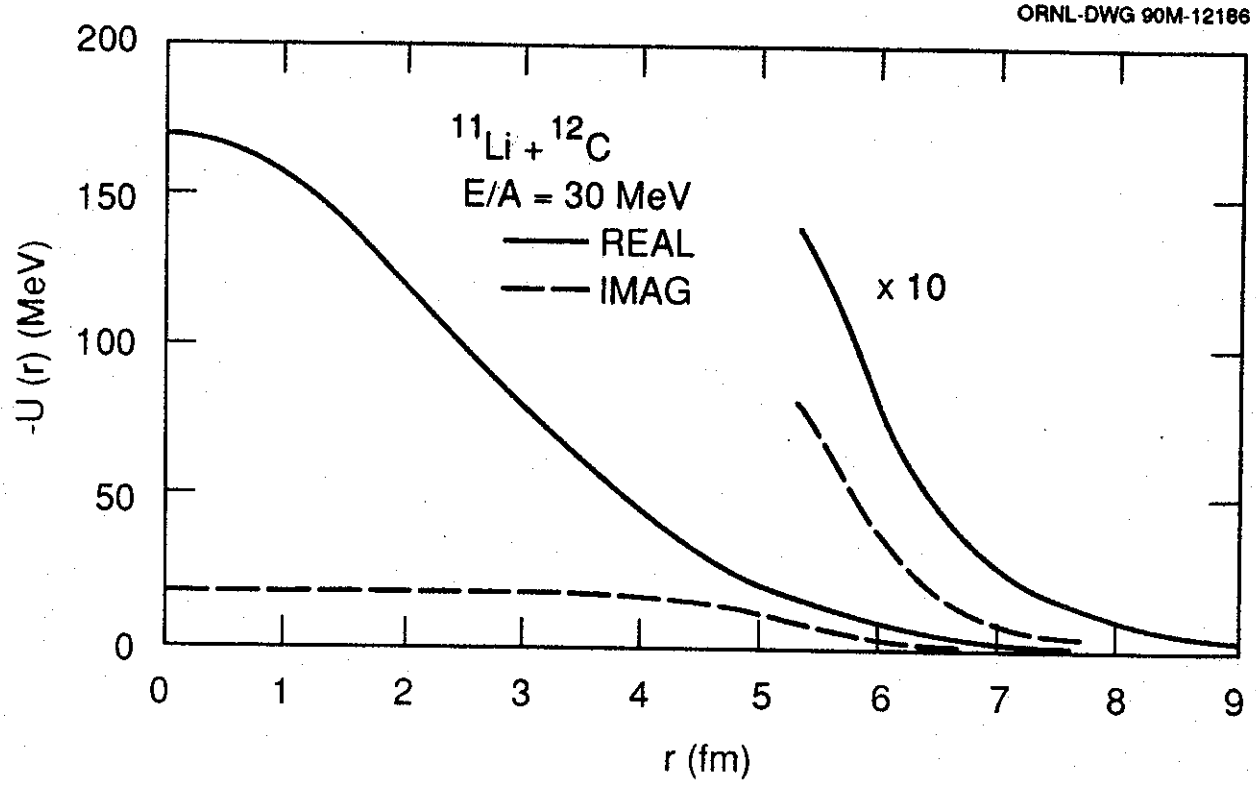
^{11}Li + ^{12}C
E/A = 30 MeV
REAL
IMAG
x 10
-U (r) (MeV)
r (fm)
200
150
100
50
0
0
1
2
3
4
5
6
7
8
9

Fig. 4

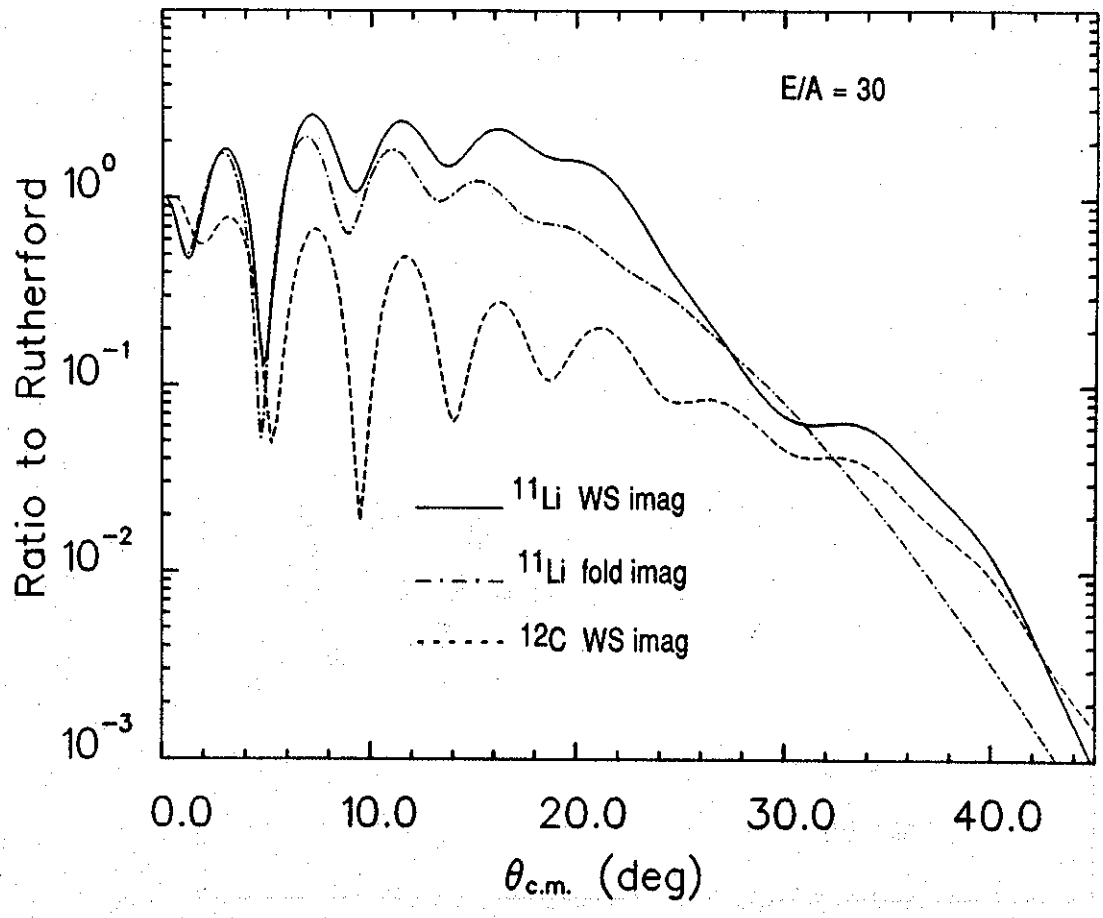
E/A = 30
Ratio to Rutherford
10^{0}
10^{-1}
10^{-2}
10^{-3}
^{11}Li WS imag
^{11}Li fold imag
^{12}C WS imag
0.0
10.0
20.0
30.0
40.0
$\theta_{c.m.}$ (deg)

Fig. 5

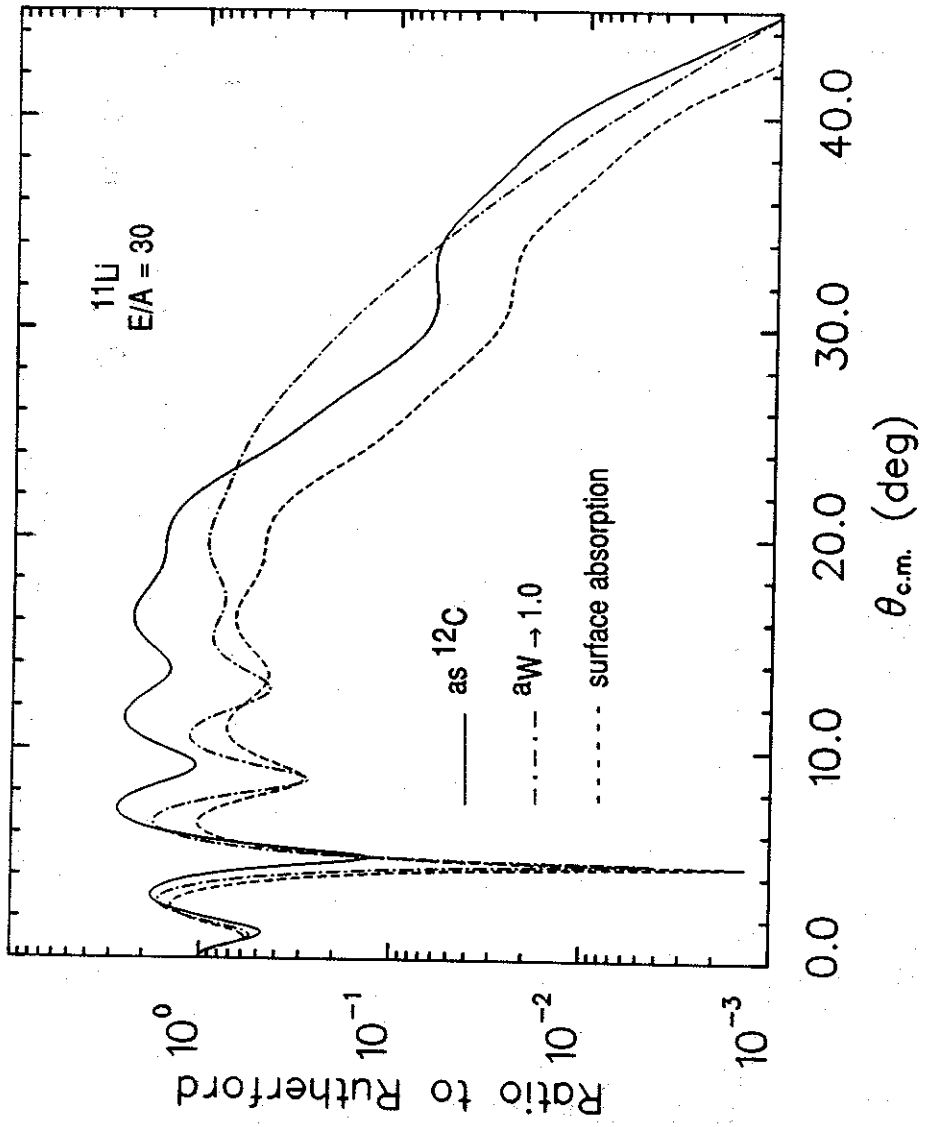
11Li
E/A = 30
as 12C
aW → 1.0
surface absorption
Ratio to Rutherford
θc.m. (deg)
10^0
10^-1
10^-2
10^-3
0.0
10.0
20.0
30.0
40.0

Fig. 6

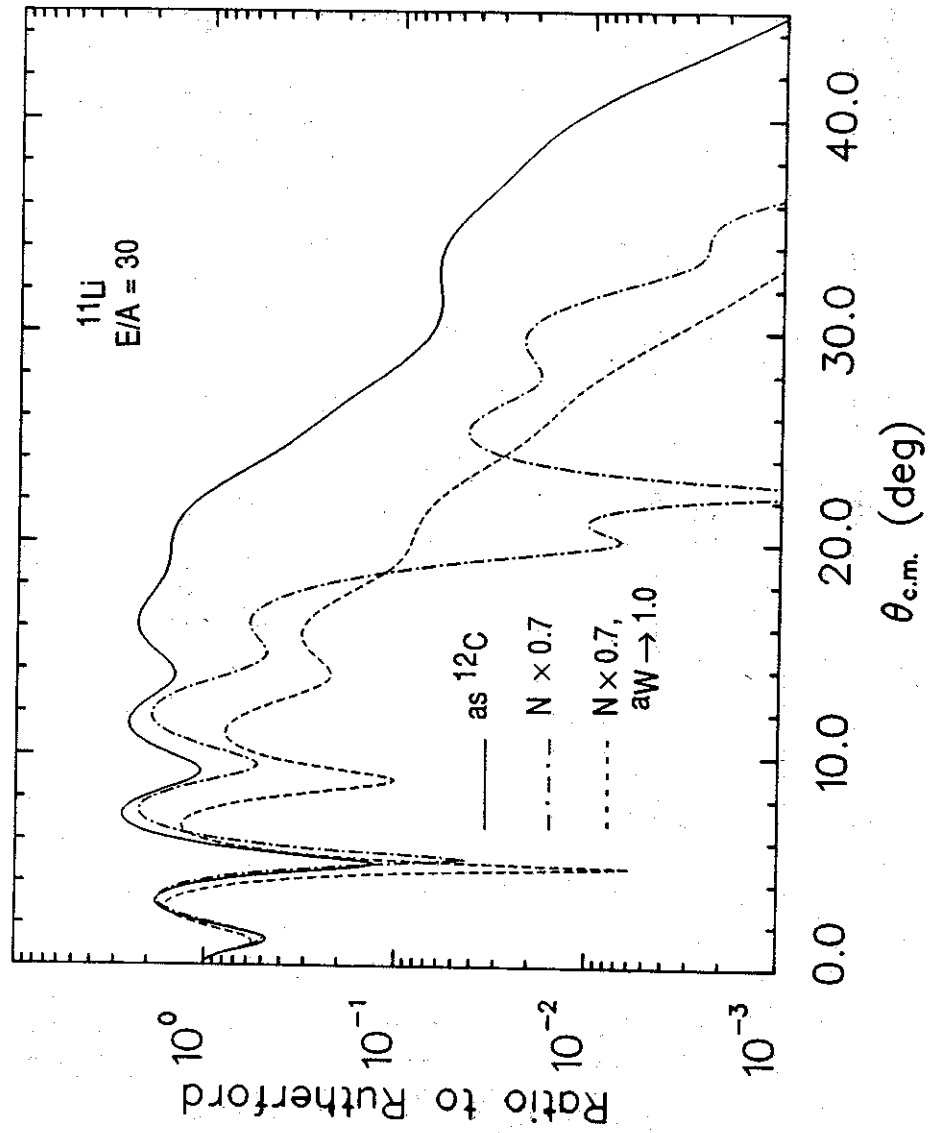
11Li
E/A = 30
as 12C
N × 0.7
N × 0.7,
aW → 1.0
Ratio to Rutherford
θc.m. (deg)
10^0
10^-1
10^-2
10^-3
0.0
10.0
20.0
30.0
40.0

Fig. 7

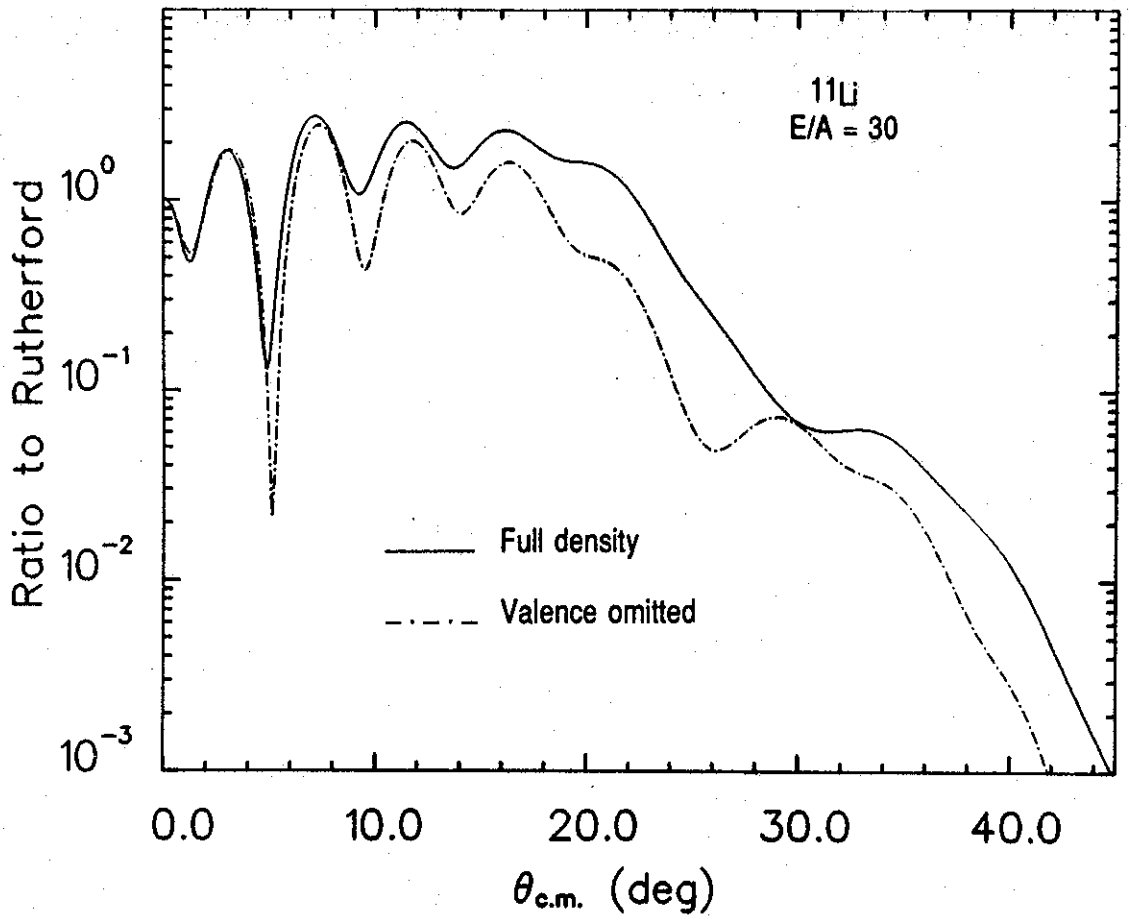
11Li
E/A = 30
Ratio to Rutherford
10^{0}
10^{-1}
10^{-2}
10^{-3}
Full density
Valence omitted
0.0
10.0
20.0
30.0
40.0
$\theta_{c.m.}$ (deg)

Fig. 8